Boundary-Layer Meteorology (2024) 190:10
https://doi.org/10.1007/s10546-023-00854-6

RESEARCH ARTICLE

A Novel Similarity Approach for Describing the Bulk Shear in the Atmospheric Surface Layer

G. H. Urbancic[1] · **I. Stiperski**[2] · **A. A. M. Holtslag**[3] · **S. Mosso**[2] · **T. Vihma**[1]

Received: 19 October 2023 / Accepted: 25 October 2023 / Published online: 4 February 2024

Abstract

The Monin–Obukhov Similarity Theory (MOST) is a cornerstone of boundary layer meteorology and the basis of most parameterizations of the atmospheric surface layer. Due to its significance for observations and modelling, we generalize the dimensional analysis of MOST by considering the bulk gradient directly, enabling the study of any sublayer of the atmospheric surface layer. This results in a family of similarity relations describing all gradients from the local gradient to the full-layer bulk gradient. By applying the profiles derived from the law-of-the-wall and MOST, we are able to derive analytic expressions for this family of similarity relations. Under stable conditions, we discover that the log-linear profile of Businger–Dyer generalizes from the local to the bulk shear where the slope is dependent on the choice of the layer. The simplicity of the general log-linear relation allows for estimating the influence of stability on the non-dimensional gradients. It is shown that bulk gradients are less sensitive to stability than the local gradient. By correctly filtering cases where the full-layer bulk gradient is influenced by stability, we demonstrate that MOST is compatible with the Hockey-Stick Transition. For unstable conditions, the Kader and Yaglom (J Fluid Mech 212(151):637-662, 1990) model represents the local gradient well but was not successful in representing the bulk gradient, demonstrating the need for further analysis of scaling relations for the unstable atmospheric surface layer.

✉ G. H. Urbancic
gabin.urbancic@fmi.fi

I. Stiperski
Ivana.Stiperski@uibk.ac.at

A. A. M. Holtslag
bert.holtslag@wur.nl

S. Mosso
samuele.mosso@uibk.ac.at

T. Vihma
timo.vihma@fmi.fi

[1] Meteorological Research, Finnish Meteorological Institute, Helsinki, Finland

[2] Department of Atmospheric and Cryospheric Science, University of Innsbruck, Innsbruck, Austria

[3] Meteorology and Air Quality Section, Wageningen University, Wageningen, The Netherlands

Keywords Atmospheric surface layer · Bulk shear · Hockey-Stick transition · Law-of-the-wall · Monin–Obukhov similarity

1 Introduction

Turbulence is the main driver for the mixing of momentum, heat, and other scalars in geophysical and engineering flows. Due to the multi-scale, complex nature of turbulent flows, the prominent challenge is to quantify how turbulence affects the mean quantities, which are the variables of interest for most applications. The first framework which can be applied to this task dates back to Boussinesq (1897), who conceptualized that the mixing ability of turbulence is analogous to viscous diffusion resulting in the eddy-viscosity model,

$$\tau = \nu_t \frac{dU}{dz}, \tag{1}$$

where $\tau = -\overline{u'w'}$ is the Reynold's stress, where u' and w' are the streamwise and normal velocity perturbations, U is the mean horizontal velocity, and ν_t is the eddy-viscosity (analogous to kinematic viscosity).

The original theory lacked a determination of ν_t which is a property of turbulence and not the fluid directly and therefore dependent on flow geometry. By drawing an analogy to kinetic theory of gases, Prandtl (1925) chose $\nu_t = l_m U_T$, where l_m is a mixing length (analogous to mean free path), and U_T is a turbulent velocity scale. Mixing length can be conceptually understood as the size of the eddies that dominate transport. Assuming the mixing length is much smaller than the scales of the mean velocity gradient (i.e. the flow consists of small-eddies), results in,

$$\nu_t = l_m^2 |\frac{dU}{dz}|. \tag{2}$$

The model becomes closed upon selection of the mixing length, l_m, and is known as mixing-length theory.

In the study of neutrally-stratified boundary layers, the pivotal discovery was made by von Kármán (1930) who hypothesized that the mixing-length is proportional to the distance from the surface, i.e $l_m = \kappa z$, where κ is the proportionality constant known as the von Kármán constant. The implication is that the size of the dominant eddies scales with the distance from the surface. Equations (1) and (2) taken together upon integration (assuming τ is constant with height) results in the law-of-the-wall,

$$\frac{U(z)}{u_*} = \frac{1}{\kappa} \ln(z) + C, \tag{3}$$

where $u_*^2 = -\overline{u'w'}$ is the velocity scale derived from the stress, known as the friction velocity, and C is a constant of integration. The law-of-the-wall shows that the velocity profile is logarithmic above the viscous sublayer.

As an alternative to mixing-length theory, dimensional analysis arrives to the same solution without the use of assumptions about the structure of turbulence to simplify the dynamic equations, and no conceptual assumption on the size of dominant eddies. The relations derived from dimensional analysis will depend on which physical parameters are chosen as relevant to the problem, thus the choice of parameters is the crux. More rigorously, the number of non-dimensional parameters is determined through the Buckingham π theorem (B-π) which states that, *given a system with n physical variables which include k physical dimensions, there* *will be $p = n - k$ non-dimensional groups which describe the system and are functionally related* (e.g. Stull 1988). For the remainder of this work we will base our presentation on B-π.

In contrast to von Kármán's initial theory which considers flow over a smooth surface, we will consider a rough surface which introduces the roughness length scale z_0, where $U(z_0) = 0$. The following set of variables are chosen for neutrally-stratified conditions,

$$\frac{dU}{dz},\ z,\ u_*, \tag{4}$$

where u_* is the friction velocity. This results in one non-dimensional group which is therefore constant, i.e.

$$\frac{z}{u_*}\frac{dU}{dz} = 1/\kappa, \tag{5}$$

where κ is chosen to match the law-of-the-wall. Upon integration, from z_0 to z, the logarithmic profile is retrieved,

$$U(z) = \frac{u_*}{\kappa}\ln\left(\frac{z}{z_0}\right). \tag{6}$$

This result is analogous to that of von Kármán for a smooth surface as it does not change the solution but exchanges the viscous length scale, defined as ν/u_*, with the roughness length-scale z_0. Although generally considered universal, the value of κ remains debated and the choice of value may result in significant differences depending on the application (George 2007). It should be noted that Eq. (5) holds even when u_* varies with height. However, u_* must be constant to allow Eq. (5) to be integrated to the logarithmic profile of the law-of-the-wall (Eq. 6).

The atmospheric boundary layer (ABL) experiences a diurnal cycle due to radiative heating and cooling of the surface. Buoyancy therefore plays a fundamental role in the structure of turbulence in the ABL. The law-of-the-wall must therefore be modified to account for effects of buoyancy. The natural extension is Monin–Obukhov Similarity Theory (MOST, Monin and Obukhov 1954), which commonly applies dimensional analysis to the following set of variables,

$$\frac{dU}{dz},\ \overline{w'\theta'},\ u_*,\ \frac{g}{\theta_0},\ z. \tag{7}$$

The turbulent fluxes (u_* and $\overline{w'\theta'}$) are both considered constant with height in MOST, referred to as the surface-layer scaling regime. The sublayer of the ABL near the surface where the fluxes are constant is known as the Atmospheric Surface Layer (ASL). When the fluxes are not constant with height, specifically under very stable conditions, the theory is valid through the local scaling framework of Nieuwstadt (1984), where the fluxes are measured at the height z. It is useful to note that the local scaling framework is a generalization of the surface-layer scaling, as it is also valid when fluxes are constant with height. Additionally, B-π produces relations which are inherently valid in the local scaling framework. However, it is not possible to integrate these relations unless the vertical profiles of the fluxes are known.

By B-π, the five parameters have three physical dimensions resulting in the following two non-dimensional groups. The first is the stability parameter,

$$\zeta = -\frac{\kappa g z}{\theta_0}\frac{\overline{w'\theta'}}{u_*^3},$$

which represents the competition between shear production of turbulence and buoyancy production/consumption. When $\zeta > 0$, $\zeta = 0$, and $\zeta < 0$, the conditions are said to be stable, neutral, and unstable, respectively. The $-\kappa$ in ζ is added for convenience to establish the relationship between ζ and the flux-Richardson number,

$$R_f = \frac{(g/\theta_0)\overline{w'\theta'}}{\overline{u'w'}(dU/dz) + \overline{v'w'}(dV/dz)},$$

i.e. ζ can be derived from R_f assuming the logarithmic wind profile (Eq. 6). The Obukhov length, L, scales the geometric height in ζ as $\zeta = z/L$. The non-dimensional gradient, $\frac{z}{u_*}\frac{dU}{dz}$, is the second non-dimensional group and is chosen to be the same as in the neutral ($\zeta = 0$) case which results in the law-of-the-wall.

The functional relationship as per B-π is:

$$\frac{z\kappa}{u_*}\frac{dU}{dz} = \phi_M(\zeta), \tag{8}$$

where ϕ_M is the universal function, determined from observations, that reduces to the law-of-the-wall when $\zeta = 0$, as $\phi_M(0) = 1$ by the definition of κ. The wind profile can be computed through integration (when fluxes are assumed constant) resulting in:

$$U(z) = \frac{u_*}{\kappa}[\ln(z/z_0) - \psi_M(z/L) + \psi_M(z_0/L)], \tag{9}$$

where ψ_M is the stability correction to the law-of-the-wall defined as:

$$\phi_M(z/L) = 1 - z\frac{\partial \psi_M(z/L)}{\partial z}. \tag{10}$$

MOST in the form of Eqs. (8) or (9) (with the addition of analogous relations for temperature, moisture and other gases) forms the basis of turbulence parameterizations in the ASL and is implemented in many weather, climate, air pollution, wind power, hydrological, and ecological models.

Although a corner stone of boundary layer meteorology, Foken (2006) ascertained that even under ideal conditions, MOST is only accurate to about 10–20%. The difficulty arises in MOST when the atmosphere is non-stationary, heterogeneous, when other length-scales are imposed on the system in addition to L, and when fluxes vary with height. Under very stable conditions, where fluxes often vary with height, the validity of scaling may be extended through the local framework of Nieuwstadt (1984), with the caveat of requiring specification of the vertical profiles of u_* and $\overline{w'\theta'}$.

In addition to the previously mentioned issues in MOST, a recent trend in research initiated by Sun et al. (2012) presents a theory known as the Hockey-Stick Transition (HOST). It is assumed in HOST that large, non-local coherent eddies are generated at wind speeds larger than a critical value and are said to mix the ASL, a phenomena which cannot be understood through the concept of local eddy-viscosity as the turbulence scales with the bulk and not the local shear. Many studies have observed HOST in their data including van de Wiel et al. (2012), Mahrt et al. (2015), Acevedo et al. (2016), and Vignon et al. (2017). Grisogono et al. (2020) extended MOST to make it compatible with HOST while Chechin (2021) argued that HOST and MOST are already compatible. Alternatively, Pfister et al. (2021) and Peltola et al. (2021) both demonstrate that HOST is a result of bin averaging different populations.

To improve the understanding of the ASL, the structure of different layers, and the length scales of the system, we generalize the dimensional analysis of MOST by considering the bulk gradient directly. The bulk gradient is important to both observations and modelling as it is commonly used for measuring turbulence and is applied as a surface flux parameterization in numerical models. The general similarity theory is derived in Sect. 2; in Sect. 3 we present the datasets which will be used to validate the theory for neutral conditions in Sect. 4 and stratified conditions in Sect. 5. The implications of the novel similarity theory on HOST is discussed in Sect. 6 followed by the conclusions in Sect. 7.

2 General Similarity Theory

To study the bulk structure of the ASL directly through a B-π approach, we generalize the following set of variables already present in MOST,

$$\overline{w'\theta'},\ u_*,\ \frac{g}{\theta_0},\ z, \tag{11}$$

by replacing the local gradient by a bulk gradient and its associated length scale,

$$\frac{U(z) - U(z - \delta z)}{\delta z},\ \delta z. \tag{12}$$

With the addition of one variable to the system, B-π requires an additional non-dimensional group. We chose the ratio of length scales, $r = \delta z / z$, which is the thickness of a layer relative to its distance to the surface. The parameter r is natural to the velocity difference in a logarithmic wind profile since:

$$\frac{U(z) - U(z - \delta z)}{u_*/\kappa} = \ln\left(\frac{z}{z_0}\right) - \ln\left(\frac{z - \delta z}{z_0}\right) = \ln\left(\frac{1}{1 - r}\right). \tag{13}$$

The three non-dimensional parameters are ζ, r, and the non-dimensional bulk gradient defined as:

$$G = \frac{z}{u_*}\frac{U(z) - U(z - \delta z)}{\delta z}. \tag{14}$$

As per the $B - \pi$, there is a functional dependence between the three non-dimensional groups i.e.,

$$G \sim \phi_G(\zeta, r). \tag{15}$$

Without loss of generality, for the neutral limit ($\zeta = 0$) we select $\phi_G(0, r) = 1$, which for $r = 0$ retrieves the law-of-the-wall. This is accomplished by multiplying a factor to G which can only be a function of r, resulting in the following family of similarity relations,

$$K(r)G = \phi_G(\zeta, r). \tag{16}$$

The function $K(r)$ can be interpreted as the normalization function of the bulk gradient during neutral conditions for a given choice of r. The height z does not completely describe the effects of a rough surface therefore an additional parameter is introduced, z_0 such that $U(z_0) = 0$, i.e the mean wind speed is zero at z_0. This additional length-scale is not fundamental as it is not part of the non-dimensional analysis but constraints the system, i.e. $\delta z \leq z - z_0$. For this study, Eq. (16) is considered in the local scaling regime, i.e. the fluxes are measured at height z to extend its validity to higher stabilities.

The two limiting cases of Eq. (16) demonstrate the range of properties described by the general similarity theory. When $r \to 0$ the local gradient relation of MOST is retrieved, i.e.

$$K(0)\frac{z}{u_*}\frac{dU}{dz} = \phi_G(\zeta, 0). \tag{17}$$

By the law-of-the-wall, $K(0)$ is therefore the von Kármán constant κ, and $\phi_G(\zeta, 0) = \phi_M(\zeta)$. In the limit where $\delta z \rightarrow z - z_0$ (the full-layer case), Eq. (16) reduces to:

$$\frac{U(z)}{u_*} = \frac{\frac{z-z_0}{z}\phi_G(\zeta, \frac{z-z_0}{z})}{K(\frac{z-z_0}{z})}, \tag{18}$$

leading to the surface stress, defined as $C_d = (u_*/U)^2$, which is a function of both stability and roughness length. The stress law is normally computed through the integration of the local gradient similarity relation (Eq. 17). By generalizing the dimensional analysis, they are both members of the same family of similarity relations.

3 Datasets and Data Processing

We use data from four multi-level turbulence towers (Table 1) located in flat and gently sloping terrain, over a range of surface roughness. The datasets include the Advective Horizontal Array Turbulence Study (AHATS, Salesky and Chamecki 2012), the Cooperative Atmosphere-Surface Exchange Study 1999 (CASES-99, Poulos et al. 2002), the NEAR tower from the Second Meteor Crater Experiment (METCRAX II, Lehner et al. 2016), and Central tower from Terrain-induced Rotor Experiment (T-Rex Central, Grubišič et al. 2008). Both AHATS and CASES-99 are over grasslands in flat, horizontally homogeneous terrain while METCRAX II and T-Rex Central are on sloping terrain over desert. Although the slope is weaker than METCRAX II, T-Rex Central observes a more complicated region as it is on a valley floor and influenced by the surrounding mountains, therefore in complex terrain. A more in-depth discussion of individual dataset characteristics can be found in Stiperski et al. (2019, 2021).

Turbulence statistics were computed using 5-min block averaging (Sun et al. 2020) for stable conditions and 30-min block averaging for unstable conditions, both with a prior linear detrending. The averaging period for stable conditions was chosen to ensure the filtering of waves in near-neutral and weakly stable conditions, while retaining the turbulent signal. We used double rotation (for AHATS, CASES-99, and T-Rex Central) and planar fit (for METCRAX II) to rotate the data, correcting for instrument misalignment and the sloping surface.

The wind speed gradients were computed from the analytically fitted mean wind speed profiles. Due to the different behaviour of each datasets (e.g., tower heights, occurrence and placement of low-level jets), the following functions were chosen: $U(z) = a + b \ln z + c(\ln z)^2$ for AHATS, $U(z) = a + bz + cz^2 + d \ln z + e(\ln z)^2$ for CASES-99 and METCRAX II, and $U(z) = a + bz + cz^2 + d \ln z$ for T-Rex Central. If the higher order fitting functions resulted in poor behaviour at the lowest observational level, a log-linear relation was applied between z_0 and that level. The roughness length for each dataset was computed from the logarithmic profile in neutral conditions ($|\zeta| < 0.02$).

To consider a regime where MOST is applicable, we removed data points with $R_f > 0.2$ following Grachev et al. (2005). As the height of the ASL varies considerably for different conditions, we considered all levels with observations to test the theory, regardless of whether or not the fluxes are constant with height. Additionally, intervals where $\overline{w'^2} > 2\ m^2/s^2$ or when missing/unreliable data exceeded 5% of points were removed from the analysis to ensure high quality data.

Table 1 Datasets used in the study

Dataset	Levels	$z_0(m)$	Slope angle (°)
AHATS	1.55, 3.3, 4.24, 5.53, 7.08, 8.05	0.014	0
CASES-99	5, 10, 20, 30, 40, 50, 55	0.0263	0
METCRAX II	3, 10, 15, 20, 25, 30, 35, 40, 45, 50	0.042	1
T-Rex Central	5, 10, 15, 20, 25, 30	0.102	0.2

4 Neutral Conditions

We chose $K(r)$ in the general similarity relation (Eq. 16) to be defined such that in neutral conditions, $\phi_G(0, r) = 1$ or $K(r) = 1/G$. Expanding G from its definition leads to:

$$K(r) = \frac{ru_*}{U(z) - U(z - \delta z)}, \tag{19}$$

and applying the law-of-the-wall results in the analytic expression:

$$K(r) = \frac{\kappa r}{\ln(\frac{1}{1-r})}. \tag{20}$$

Consistent with the definition of $K(r)$, the von Kármán constant is retrieved in the limit $r \rightarrow 0$ by applying L'Hopital's rule, i.e $\lim_{r \to 0} K(r) = \kappa$. Figure 1 presents the bin averaged $K(r)$ values computed from all four datasets and for all measurement height combinations by normalizing the non-dimensional gradient during neutral conditions (as seen in Fig. 2). The law-of-the-wall successfully explains the observed bulk structure of the ASL during neutral conditions.

The von Kármán constant κ is computed from the data through regression to Eq. (20), and ranges from 0.30 to 0.37. The von Kármán constant can also be computed directly by normalizing the local gradient ($r = 0$), which as seen in the bin averaged values in Fig. 1 does not result in significant differences. The advantage of applying Eq. (20) to compute κ is to remove the sensitivity of the local gradient calculation on the estimation of κ. Our values for AHATS, CASES-99, and T-Rex Central are smaller than the range of 0.35−0.43 reported in Foken (2006) and smaller than most values reported in Högström (1996). The smallest value is for T-Rex Central which exhibits $\kappa = 0.30$. Deviations for T-Rex Central can be associated to the effects of complex terrain on scaling and have been investigated in Babić et al. (2016b). Although deviating from canonical conditions, T-Rex Central fits Eq. (20) as well as the datasets which are closer to canonical just with a lower κ. Although treated identically as the other datasets, CASES-99 exhibits poor behaviour, most likely due to measurement or processing error.

Interestingly, all four datasets converge quite well on the upper domain of r as seen in the sub-panel of Fig. 1. The κ predicted by the upper domain ($r > 0.99$) is around 0.38, which we use for this study. The von Kármán constant, as measured through the whole r domain, varies considerably. Local and non-local processes, heterogeneity, and the effects of complex terrain result in deviations from the law-of-the-wall, which could contribute to the observed variations between the datasets. Variations between the κ values computed in this study and those presented in earlier literature is most likely a result of improvements in flux measurement and processing techniques. A thorough investigation of the sensitivity of κ to different methods is warranted but beyond-the-scope of this work.

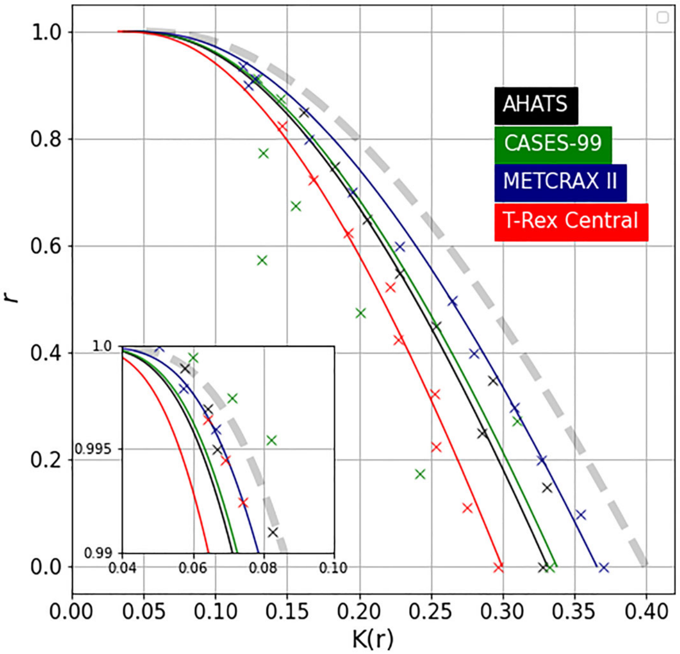

Fig. 1 The bin averaged values (x symbols) of $K(r)$ for various datasets. The solid curves are the regression to Eq. (20) for κ for each dataset. The dashed curve shows the theoretical curve for $\kappa = 0.4$

5 Stratified Conditions

To consider stratified conditions ($\zeta \neq 0$) analytically, $\phi_G(\zeta, r)$ can be expressed in terms of the $\psi_M(\zeta)$ function from MOST, which is the deviation from the law-of-the-wall (Eq. 10). First, the non-dimensional bulk gradient, G, is expanded from its definition in Eq. (16) and applying the analytic $K(r)$ derived from the law-of-the-wall (Eq. 20), results in:

$$\phi_G(\zeta, r) = \frac{\kappa}{\ln(\frac{1}{1-r})} \frac{U(z) - U(z - \delta z)}{u_*}. \tag{21}$$

The wind profile, $U(z)$, is then selected to be the stability-modified wind profile of MOST (Eq. 9), which results in the MOST prediction of ϕ_G,

$$\phi_G(\zeta, r) = 1 - \frac{\psi_M(\zeta) - \psi_M(\zeta(1-r))}{\ln(\frac{1}{1-r})}. \tag{22}$$

Ultimately, it is possible to determine empirically whether MOST, via the selection of ψ_M, is effective in representing the non-dimensional bulk gradient ϕ_G.

5.1 Stable Conditions

The Businger–Dyer relation for stable conditions is $\psi_M = -\beta\zeta$, where $\beta \approx 5$ (Högström 1996). Applying Businger–Dyer to Eq. (22) results in the general log-linear relation,

$$\phi_G(\zeta, r) = 1 + \beta \frac{K(r)}{\kappa} \zeta. \tag{23}$$

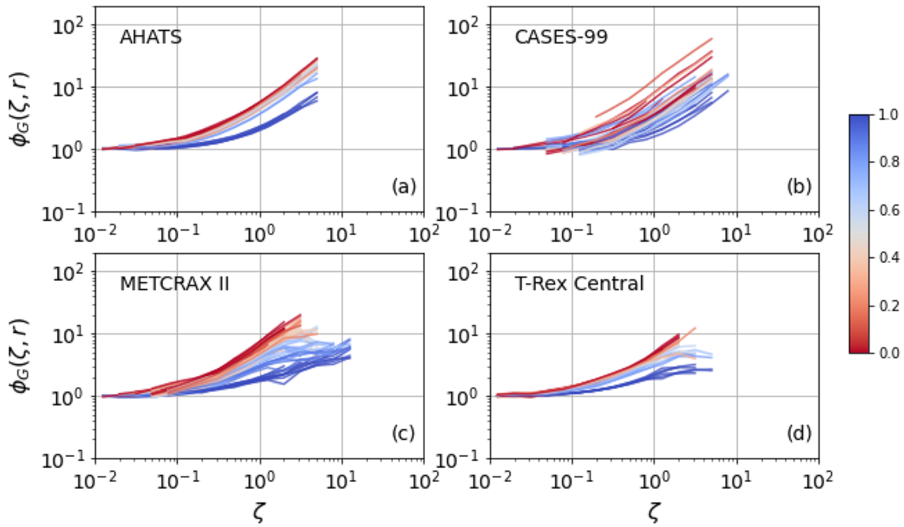

Fig. 2 The similarity curves for stable conditions of the bulk gradient for **a** AHATS, **b** CASES-99, **c** METCRAX II, and **d** T-Rex Central. All possible separations (δz) are considered with each curve colour coded by its r value, blue for the full-layer bulk gradient and red for the local gradient

It should be noted that having a log-linear wind profile is the only relation which is form preserving in Eq. (22). The similarity curves, ϕ_G, are presented in Fig. 2 for all possible r values, i.e. every combination of the measurement heights. With the exception of CASES-99 which behaves poorly, the data shows log-linear behaviour with large values of r exhibiting a delayed onset of the influence of stability (i.e. the curves with larger r deviate from $\phi_G \approx 1$ at larger ζ).

To test the validity of the general log-linear relation, Eq. (23) is rearranged to separate out the dependence on r, i.e

$$\frac{\phi_G(\zeta, r) - 1}{K(r)/\kappa} = \beta\zeta. \tag{24}$$

The bin averaged medians for each dataset, which include every instrument height and possible separation (δz), are plotted in Fig. 3. All the datasets collapse extremely well to the generalized log-linear relation with $\beta = 5$ for $\zeta < 2$. The datasets over flat terrain (AHATS, CASES-99) have extended validity and are valid up to $\zeta \approx 10$. Variations becomes excessive at large stability matching the already understood limitations of MOST for such conditions, i.e when turbulence is non-stationary, non-Kolmogorov, highly anisotropic, and/or intermittent (e.g. Grachev et al. 2013, Babić et al. 2016a).

The dependence of ϕ_G on stability can be treated from the general log-linear relation. The slope in Eq. (23) is independent of the von Kármán constant, and its dependence on r only originates from $K(r)$. As $K(r)$ is a monotonically decreasing function of r, an immediate consequence is that the stability dependence of ϕ_G is weaker for larger values of r as already demonstrated in Fig. 2. The full-layer bulk gradient ($\delta z = z - z_0$) is therefore more robust to stability than the local gradient ($\delta z = 0$).

A threshold for when stability has significantly influenced ϕ_G can be derived from the general log-linear relation. We chose the threshold as the value of ζ for which ϕ_G is 50% larger than its neutral value, i.e. $\phi_G = 1.5$. Applying Eq. (23) with $\beta = 5$, and setting

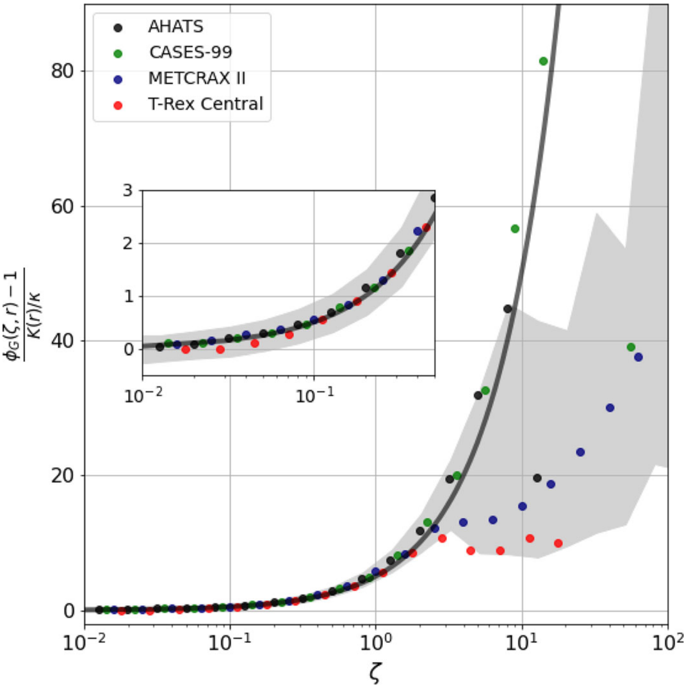

Fig. 3 The scaled (for r) stability curves of the bulk gradient for each datasets using all possible separations (δz). The black line is the generalized log-linear relation with $\beta = 5$. The shaded region shows the range between the 25^{th} and 75^{th} percentile for the full dataset

$\phi_G = 1.5$ results in:

$$\zeta_t(r) = \frac{\kappa}{2\beta K(r)} = \frac{\ln(\frac{1}{1-r})}{10r}. \tag{25}$$

For the local gradient ($r = 0$), the threshold is $\zeta_t(0) = 0.1$, which coincides with the upper limit for the weakly stable regime of Grachev et al. (2005), defined as the regime where u_* and $\overline{w'\theta'}$ are approximately constant with height. Considering the upper limit of r and taking $z = 10$ m as an example (i.e. $\delta z = 10 - z_0$), ζ_t ranges from 0.46 to 0.66 due to variations in z_0 (Table 1). A larger z_0 (as observed in T-Rex Central) leads to a smaller value of r and consequently a smaller ζ_t. Compared to the $\zeta_t(0) = 0.1$ of Grachev et al. (2005), there is a factor of 4.6 to 6.6 increase in ζ_t for the full-layer bulk. This implies that for the datasets considered in this study, the full-layer bulk gradient through the lowest 10 m's is robust to stability for a 4.6 to 6.6 larger domain of ζ than the local gradient at 10 m.

5.2 Unstable Conditions

Applying the stability correction function for unstable conditions from Brutsaert (1992),

$$\psi_M = \frac{1-b}{n} \ln\left(\frac{a + |\zeta|^n}{a}\right) - 3c|\zeta|^{1/3}, \tag{26}$$

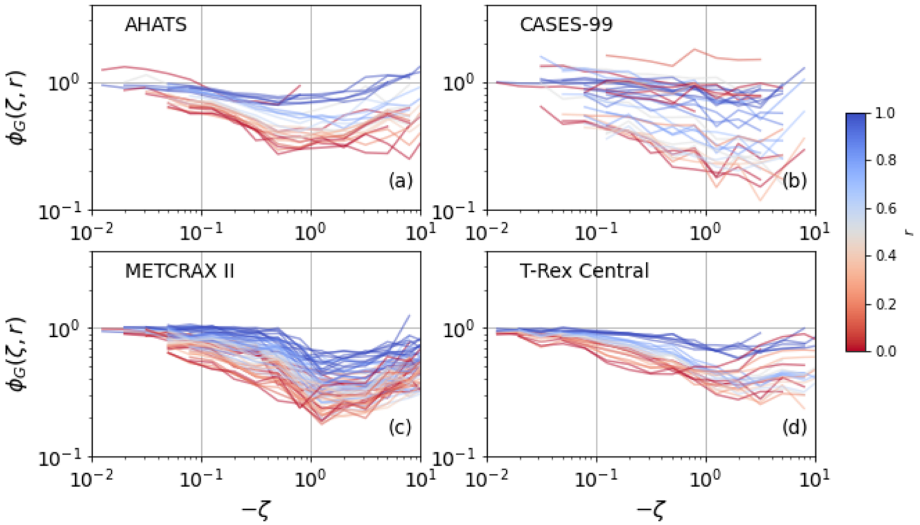

Fig. 4 The similarity curves for unstable conditions of the bulk gradient for **a** AHATS, **b** CASES-99, **c** METCRAX II, and (4) T-Rex Central. All possible separations (δz) are considered with each curve colour coded by its r value, blue for the full-layer bulk gradient and red for the local gradient

which is based on the Kader and Yaglom (1990) model, results in the following similarity relation,

$$\phi_G(\zeta, r) = 1 - \frac{1}{\ln \frac{1}{1-r}} \left\{ \frac{1-b}{n} \ln \left(\frac{a + |\zeta|^n}{a + |\zeta|^n (1-r)^n} \right) - 3c|\zeta|^{1/3}(1 - (1-r)^{1/3}) \right\}. \tag{27}$$

The Kader and Yaglom (1990) model differs from the Businger–Dyer relations and analytical solutions of the O'KEYPS equation (e.g. Li 2021) by predicting an increase in ϕ_M for $\zeta < -1$, instead of a monotonically decreasing behaviour. The increasing ϕ_M is consistent with measurements (see Fig. 4).

The non-linearity of the stability correction function for unstable conditions inhibits a result as simple as Eq. (23) and the effects of ζ and r on ϕ_G are not separable as is the case for stable conditions (Eq. 24). This implies the collapse of the curves in Fig. 3 is not possible for the full range of unstable ζ values. The ϕ_G function based on Brutsaert (1992) with the original parameter values is plotted in Fig. 5a as well as the curve fits for the four datasets. Values of a, b, c and n for each is presented in Table 2. Rearranging ϕ_G in same form as Eq. (24) shows an approximate collapse of the curves when $\zeta > -0.2$ (Fig. 5b). This collapse occurs for the Brutsaert (1992) values as well as for the four datasets (not shown), and corresponds to the transition from the dynamic-convective to dynamic sublayers of the Kader and Yaglom (1990) model. The results suggest that the dependence of ϕ_G on ζ and r is not separable during unstable conditions when buoyancy production is comparable-to or larger-than the dynamical production of turbulence.

Figure 4 shows ϕ_G for all possible values of r for the four datasets. Similar to stable conditions, the bulk gradients are more robust to stratification than the local gradients. The lack of collapse of the curves with the same r is indicative of missing parameters to the problem as discussed in Salesky and Chamecki (2012). As seen in Fig. 5, the analytic curves from Eq. (27) show a reverse in ordering at around $\zeta = -1$. This was not observed in the

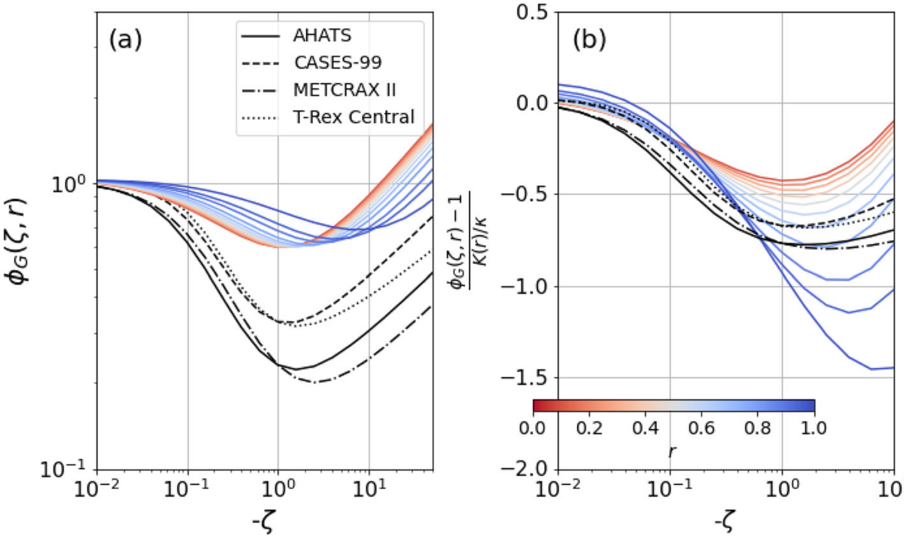

Fig. 5 The analytic similarity curves of the bulk gradient for unstable conditions (Eq. 27). Each coloured curve is Eq. (27) with the parameter values from Brutsaert (1992) and is coded by its r value, blue for the full-layer bulk gradient and red for the local gradient. The black curves are the curve fits to AHATS, CASES-99, METCRAX II and T-Rex Central for $r = 0$

Table 2 Parameters of the ψ_M function of Brutsaert 1992 (Eq. 26) from the original study and from AHATS, CASES-99, METCRAX II, and T-Rex Central

	a, b, c, n
Brutsaert (1992)	0.37, −0.24, 0.50, 0.72
AHATS	0.08, 0.04, 0.12, 1.18
CASES-99	0.09, 0.06, 0.19, 1.29
METCRAX II	0.12, 0.037, 0.091, 1.11
T-Rex Central	0.084, 0.14, 0.12, 1.43

datasets with exception of T-Rex Central, implying the ψ_M considered is not reconstructing ϕ_G universally. In contrast to stable conditions, the four datasets exhibit different properties for unstable conditions, including the minimum values of ϕ_G and the transition from dynamic to dynamic-convective conditions. This can also be seen in the range of values presented in Table 2. This analysis demonstrates that the bulk shear similarity, as treated in this study, was not successful in explaining the observations and indicates the need for further work on the scaling relations of the bulk shear in the unstable ASL.

6 Implications for the Hockey-Stick Transition

The Hockey-Stick Transition (HOST), developed by Sun et al. (2012, 2016), states that there are two distinct regimes observed in $U_T - U$ space (e.g. Figure 6a), where U_T is a turbulent velocity scale. For weak winds, U_T exhibits a weak dependence on wind speed until a critical wind speed (U_{Ho}) is reached where the relation becomes linear, i.e. $U_T \sim U$. The branch where $U < U_{Ho}$ is considered stable while $U > U_{Ho}$ is considered neutral. The threshold between the two, U_{Ho}, increases with the measurement height while the slope for $U > U_{Ho}$

is considered constant with height. Physically, the threshold is interpreted as the wind speed whereupon large, non-local coherent eddies are generated which mix the ASL.

We address two contradictions between HOST and the law-of-the-wall, which by relation implies a contradiction with MOST. Firstly, HOST claims that for the so-called neutral branch, extending the linear trend to the low wind speed limit results in a negative U_T. Secondly, the slopes of the neutral branch are constant with height. The law-of-the-wall (Eq. 6), for which u_* is taken as U_T, gives the following $u_* - U$ relation,

$$u_* = \frac{\kappa}{\ln(z/z_0)} U. \tag{28}$$

We can see from Eq. (28) that $\lim_{U \to 0} u_* = 0$, and the slope is dependent on height through z/z_0, contradicting HOST. We will demonstrate that the contradictory features are a result of erroneously identifying the $U > U_{Ho}$ of HOST as the neutral branch.

The bin averaged $U_T - U$ relations during stable conditions for the four datasets are presented in Fig. 6, for which u_* is chosen as U_T. Figure 6(c, d) shows the CASES-99 dataset which was used for the original study of HOST (Sun et al. 2012). When examining the full dataset, the shape of the curves (left column) resembles a hockey stick where the lower branch shows a weak dependence on wind speed until a certain wind speed (U_{Ho}), where the curve transitions to a steeper slope. The region with a steeper slope does not coincide with the law-of-the-wall, which predicts a range of straight lines (shown in grey) due to dependence on z/z_0.

As HOST considers the data in $u_* - U$ space, then the relevant ϕ_G is for the full layer with $\delta z = z - z_0$ as it provides the relation between U and u_* (Eq. 18). We demonstrated in Sect. 5.1 that separating regimes through ζ depends on which layer is considered. For the full layer, the ζ value for which ϕ_G is 50% larger than its neutral value is:

$$\zeta_t^{z_0} = \zeta_t \left(\frac{z - z_0}{z} \right) = \frac{z \cdot \ln(z/z_0)}{10(z - z_0)}. \tag{29}$$

We therefore apply $\zeta_t^{z_0}$ to separate cases where stability has significantly (by 50%) modified ϕ_G and the cases for which it has not. The curves with $\zeta < \zeta_t^{z_0}$ and $\zeta > \zeta_t^{z_0}$ are presented in the right column of Fig. 6. For $\zeta < \zeta_t^{z_0}$, the curves show slopes which mostly fall in the range predicted by the law-of-the-wall. The slight variations from the law-of-the-wall are likely a result of weak stability, instrument errors and uncertainty in the computation of z_0. For low wind speeds, the u_* values for $\zeta < \zeta_T^{z_0}$ approach a positive, non-zero value which is contradictory to both HOST and MOST, and is attributed to submeso scale motions (e.g. Urbancic et al. 2020). For $\zeta > \zeta_t^{z_0}$, the different levels exhibit a weakly increasing curve that significantly overlaps in the wind speed domain with the $\zeta < \zeta_t^{z_0}$ case. This curve is not physically insightful as it involves the bin-averaging of points with a wide range of stabilities and properties. Regardless, as seen in the left column, the values of the lower branch extend to much larger wind speeds than U_{Ho}. For example, the CASES-99 data at 40 m has U_{Ho} occurring at around 6 m/s while stable cases occur up to 9 m/s. We conclude that wind speeds larger than U_{Ho} do not necessarily result in the transition to a neutral conditions since the neutral branch of HOST is not exclusively derived from neutral conditions. Furthermore, our results demonstrate that HOST is an artifact of bin-averaging distinct populations.

The two branches in $u_* - U$ space, as described by HOST (left column in Fig. 6), do not identify features which are incompatible with MOST as their properties depend on the distribution of ζ. For example, the value of U_{Ho} depends on the population of points in each stability bin and is therefore not a physical constant. This may explain the variations in U_{Ho} between different sites discussed in Acevedo et al. (2021). The increase in U_{Ho} for different

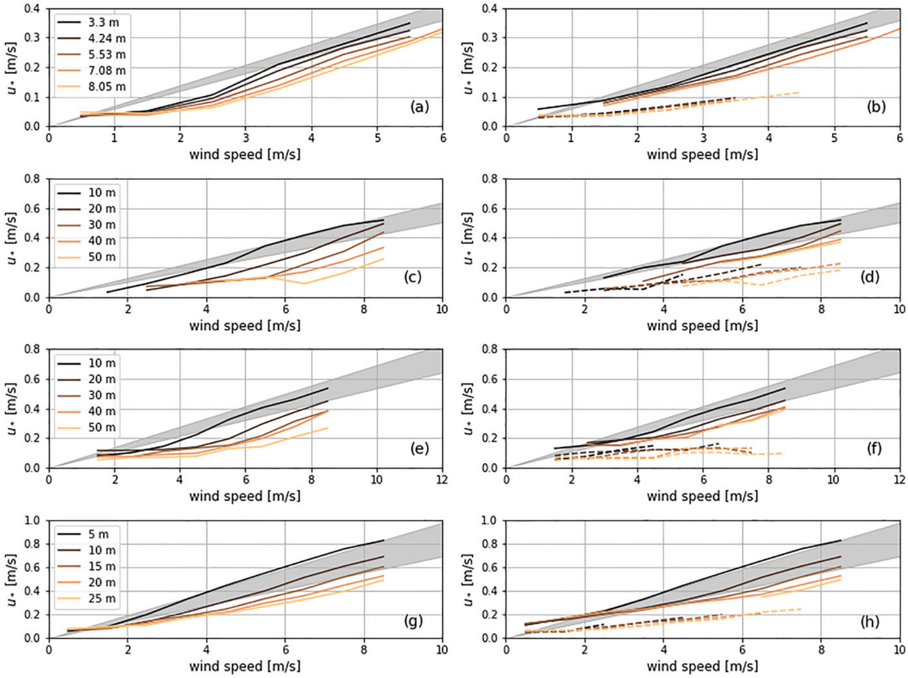

Fig. 6 The u_*–U curves for (**a**, **b**) AHATS, (**c**, **d**) CASES-99, (**e**, **f**) METCRAX II, and (**g**, **h**) T-Rex Central. Left column (**a**, **c**, **e**, **g**) show the bin average for the full dataset while the right column (**b**, **d**, **f**, **h**) show the bin average for $\zeta < \zeta_t$ (solid) and $\zeta > \zeta_t$ (dashed). The shaded grey region shows the range expected from the log-wind profile, i.e. for neutral conditions, for the range of heights considered

heights can be simply attributed to an increase in ζ as $\zeta \sim z$, altering its distribution, as well as a decrease in u_* occurring with height, as commonly observed in the SBL. If the weakly-stable condition ($\zeta < 0.1$) of Grachev et al. (2005) was applied instead of ζ_T^{z0}, then points which are not significantly influenced by stability ($0.1 < \zeta < \zeta_T^{z0}$) would affect the statistics of the stable branch resulting in a variant of HOST. Both Pfister et al. (2021) and Peltola et al. (2021) also demonstrate that HOST is an artifact of bin-averaging by separating the data into two populations by their position in relation to thermal submesofronts and by being in coupled and decoupled states, respectively. Therefore, U_{Ho} is not a physical prognostic of the ASL.

The approach of explaining HOST as an artifact of bin-averaging populations with different properties is not contradictory to Chechin (2021), who showed that MOST can recreate the HOST. Chechin (2021) applied Eq. (9) to extract the $u_* - U$ relation by empirically setting L as a function of u_* through bin-averaging. This approach still treats the full population of points irrespective of ζ, naturally resulting in HOST.

7 Conclusions

To investigate the structure of bulk shear in the ASL we generalize MOST from the local gradient to a bulk gradient. This generalized approach results in a practical and therefore elegant family of similarity relations. Through this theory, we can establish the similarity of different shear layers in the ASL based on the thickness of the layer relative to its height above the surface. The seamless transition through this family of similarity relations, from the scaling of the local gradient to the full-layer bulk gradient, demonstrates the unified identity of these variables. Care should therefore be taken when considering the bulk and local gradients as competing influences on the ASL.

Under neutral conditions, the normalization function of the non-dimensional bulk gradient, $K(r)$, can be thought of as a von Kármán function and is correctly predicted by the logarithmic wind profile of the law-of-the-wall. The von Kármán constant, κ, is the limiting case of $K(r)$ for a local gradient ($r = 0$) and once known, fully defines the $K(r)$ function. As the other limit (full-layer case) is not universal, due to dependence on z_0, it is clear that the local gradient is in-fact the natural variable of consideration as it is through the local gradient that the universal constant κ is found. If HOST was correct in saying that the slope of $u_* - U$ was constant during neutral conditions and independent of height, then a new constant, other than κ, would be extracted in the observed $K(r)$ function. However, this was not the case in our data which obeys the law-of-the-wall.

Under stable conditions, we determined that the log-linear relation of Businger–Dyer in the stable boundary layer can be generalized to all bulk gradients (Eq. 23), where the constant slope is a function of r. This allows for quantifying the influence of stability on the bulk gradients and to demonstrate how this dependence varies on the choice of r. The full-layer bulk gradient (and by association the surface stress) is considerably more robust to stability than the local gradient. By taking this into account in the threshold value of ζ (Eq. 29) we are able to correctly filter the data influenced by stability to demonstrate that MOST is compatible with HOST. We also show that high stability cases also occur under moderate to high wind speeds. There is therefore no critical wind speed threshold where large, non-local coherent eddies become significant and mix the ASL. Therefore, it seems likely eddies of all sizes contribute to establishing the wind speed profile of the ASL.

For unstable conditions, ϕ_G assumes a complicated analytical form due to the non-linear dependency on ζ of the stability correction functions. This non-linearity prevents the separation of the influence of r and ζ in the dynamic-convective and free convective sublayers of the Kader and Yaglom (1990) model, making the situation more complicated than in stable conditions. Additionally, the non-dimensional bulk gradient, G, is not fully described by ζ and r implying the need to introduce more parameters to the dimensional analysis. For all datasets, we observed non-monotonic behaviour at large values of $-\zeta$ which is not represented in the Businger–Dyer relation but predicted by the model of Kader and Yaglom (1990). The stability correction function from Brutsaert (1992), which is based on the Kader and Yaglom (1990) model, does not successfully represent the bulk gradient. Further analysis on the scaling relations of the unstable atmospheric surface layer is warranted.

The Monin–Obukhov Similarity Theory remains the foundational theory explaining the structure of the atmospheric surface layer. Improvements and extensions are needed to increase the regimes of its validity. Promising advances are under way including taking into account the anisotropy of the system, extending the work of Stiperski and Calaf (2018, 2021, 2022), and/or machine learning methods (e.g. McCandless et al. 2022) which may represent processes which are not easily accessible through classical theory.

Acknowledgements This work was supported by the Vilho, Yrjö, and Kalle Väisälä Scholarship (Urbancic); and the European Research Council (ERC) with Grant agreement No. 101001691 under the European Union's Horizon 2020 research and innovation program (Stiperski).

Author Contributions G.U. devised the study, conceived/derived the theory, wrote the manuscript, and prepared the figures. I.S prepared the datasets used in the study. I.S. and B.H. strongly contributed to the theory development, result interpretation, and manuscript writing. S.M. contributed to theory development, result interpretation, and manuscript writing. T.V. contributed to the result interpretation, manuscript writing, and generally supported the study.

Funding Open access funding provided by Finnish Meteorological Institute.

Declarations

Conflict of interest The authors declare no competing interests.

References

Acevedo O, Mahrt L, Puhales F, Costa F, Medeiros L, Degrazia G (2016) Contrasting structures between the decoupled and coupled states of the stable boundary layer. Q J R Meteorol Soc 142(695):693–702. https://doi.org/10.1002/qj.2693

Acevedo OC, Costa FD, Maroneze R, Carvalho AD, Puhales FS, Oliveira PE (2021) External controls on the transition between stable boundary-layer turbulence regimes. Q J R Meteorol Soc 147(737):2335–2351. https://doi.org/10.1002/qj.4027

Babić K, Rotach MW, Klaić ZB (2016a) Evaluation of local similarity theory in the wintertime nocturnal boundary layer over heterogeneous surface. Agric For Meteorol 228:164–179

Babić N, Večenaj Ž, De Wekker SF (2016b) Flux-variance similarity in complex terrain and its sensitivity to different methods of treating non-stationarity. Bound-Layer Meteorol 159:123–145

Boussinesq J (1897) Théorie de l'écoulement tourbillonnant et tumultueux des liquides dans les lits rectilignes a grande section, vol 1. Gauthier-Villars

Brutsaert W (1992) Stability correction functions for the mean wind speed and temperature in the unstable surface layer. Geophys Res Lett 19(5):469–472

Chechin D (2021) On the u_*–U relationship in the stable atmospheric boundary layer over arctic sea ice. Atmosphere 12(5):591

Foken T (2006) 50 years of the Monin-Obukhov similarity theory. Bound-Layer Meteorol 119(3):431–447. https://doi.org/10.1007/s10546-006-9048-6

George WK (2007) Is there a universal log law for turbulent wall-bounded flows? Philos Trans R Soc A: Math, Phys Eng Sci 365(1852):789–806. https://doi.org/10.1098/rsta.2006.1941

Grachev A, Fairall C, Persson P, Andreas E, Guest P (2005) Stable boundary-layer scaling regimes: the SHEBA data. Bound-Layer Meteorol 116(2):201–235. https://doi.org/10.1007/s10546-004-2729-0

Grachev A, Andreas E, Fairall C, Guest P, Persson P (2013) The critical Richardson number and limits of applicability of local similarity theory in the stable boundary layer. Bound-Layer Meteorol 147(1):51–82. https://doi.org/10.1007/s10546-012-9771-0

Grisogono B, Sun J, Belušić D (2020) A note on MOST and HOST for turbulence parametrization. Q J R Meteorol Soc 146(729):1991–19971. https://doi.org/10.1002/qj.3770

Grubišič V, Doyle JD, Kuettner J, Dirks R, Cohn SA, Pan LL, Mobbs S, Smith RB, Whiteman CD, Czyzyk S, Vosper S, Weissmann M, Haimov S, Wekker SFJD, Chow FK (2008) The Terrain-induced rotor experiment. Bull Am Meteor Soc 89(10):1513–1533

Högström U (1996) Review of some basic characteristics of the atmospheric surface layer. Bound-Layer Meteorol 78(3–4):215–246. https://doi.org/10.1007/BF00120937

Kader BA, Yaglom AM (1990) Mean fields and fluctuation moments in unstably stratified turbulent boundary layers. J Fluid Mech 212(151):637–662. https://doi.org/10.1017/S0022112090002129

Lehner M, Whiteman CD, Hoch SW, Crosman ET, Jeglum ME, Cherukuru NW, Calhoun R, Adler B, Kalthoff N, Rotunno R, Horst TW, Semmer S, Brown WOJ, Oncley SP, Vogt R, Grudzielanek AM, Cermak J, Fonteyne NJ, Bernhofer C, Pitacco A, Klein P (2016) The METCRAX II field experiment: a study of downslope windstorm-type flows in Arizona's Meteor Crater. Bull Am Meteor Soc 97:217–235

Li D (2021) The O'KEYPS equation and 60 years beyond. Bound-Layer Meteorol 179(1):19–42

Mahrt L, Sun J, Stauffer D (2015) Dependence of turbulent velocities on wind speed and stratification. Bound-Layer Meteorol 155(1):55–71. https://doi.org/10.1007/s10546-014-9992-5

McCandless T, Gagne DJ, Kosović B, Haupt SE, Yang B, Becker C, Schreck J (2022) Machine learning for improving surface-layer-flux estimates. Bound-Layer Meteorol 185(2):199–228. https://doi.org/10.1007/s10546-022-00727-4

Monin A, Obukhov A (1954) Basic laws of turbulent mixing in the surface layer of the atmosphere. Contrib Geophys Inst Acad Sci USSR 151(163):163–187

Nieuwstadt FTM (1984) The turbulent structure of the stable. Nocturnal Boundary Layer. https://doi.org/10.1175/1520-0469(1984)041<2202:TTSOTS>2.0.CO;2

Peltola O, Lapo K, Thomas CK (2021) A physics-based universal indicator for vertical decoupling and mixing across canopies architectures and dynamic stabilities. Geophys Res Lett 48(5):1–11. https://doi.org/10.1029/2020GL091615

Pfister L, Lapo K, Mahrt L, Thomas CK (2021) Thermal Submeso motions in the nocturnal stable boundary layer. Part 2: generating mechanisms and implications. Boundary-Layer Meteorol 180(2):203–224. https://doi.org/10.1007/s10546-021-00619-z

Poulos GS, Blumen W, Fritts DC, Lundquist JK, Sun J, Burns SP, Nappo C, Banta R, Newsom R, Cuxart J, Terradellas E, Balsley B, Jensen M (2002) CASES-99: a comprehensive investigation of the stable nocturnal boundary layer. Bull Am Meteor Soc 83(4):555–581

Prandtl L (1925) Bericht über Untersuchungen zur ausgebildeten Turbulenz. ZAMM - J Appl Math Mech / Zeitschrift für Angewandte Mathematik und Mechanik 5(2):136–139

Salesky ST, Chamecki M (2012) Random errors in turbulence measurements in the atmospheric surface layer: implications for monin-obukhov similarity theory. J Atmos Sci 69(12):3700–3714

Stiperski I, Calaf M (2018) Dependence of near-surface similarity scaling on the anisotropy of atmospheric turbulence. Q J R Meteorol Soc 144(712):641–657. https://doi.org/10.1002/qj.3224

Stiperski I, Calaf M (2021) Universal return to isotropy of inhomogeneous atmospheric boundary layer turbulence. Phys Rev Lett 126(19):194501. https://doi.org/10.1103/PhysRevLett.126.194501

Stiperski I, Calaf M (2022) Generalizing Monin-Obukhov similarity theory (1954) for complex atmospheric turbulence. Phys Rev Lett 130(12):124001. https://doi.org/10.1103/PhysRevLett.130.124001

Stiperski I, Calaf M, Rotach MW (2019) Scaling, anisotropy, and complexity in near-surface atmospheric turbulence. J Geophys Res Atmos 124:1428–1448

Stiperski I, Chamecki M, Calaf M (2021) Anisotropy of unstably stratified near-surface turbulence. Bound-Layer Meteorol 180(3):363–384

Stull RB (1988) An introduction to boundary layer meteorology, vol 13. Springer, Germany

Sun J, Mahrt L, Banta R, Pichugina Y (2012) Turbulence regimes and turbulence intermittency in the stable boundary layer during CASES-99. J Atmos Sci 69(1):338–351. https://doi.org/10.1175/JAS-D-11-082.1

Sun J, Lenschow DH, LeMone MA, Mahrt L (2016) The Role of large-coherent-eddy transport in the atmospheric surface layer based on CASES-99 observations. Bound-Layer Meteorol 160(1):83–111. https://doi.org/10.1007/s10546-016-0134-0

Sun J, Takle E, Acevedo O (2020) Understanding physical processes represented by the Monin - Obukhov bulk formula for momentum transfer. Bound-Layer Meteorol. https://doi.org/10.1007/s10546-020-00546-5

Urbancic G, Suomi I, Vihma T (2020) A general theory for the characterization of submeso-scale motions and turbulence in the atmospheric surface layer. Q J R Meteorol Soc 147(734):660–678. https://doi.org/10.1002/qj.3939

van de Wiel B, Moene A, Jonker H, Baas P, Basu S, Donda J, Sun J, Holtslag A (2012) The minimum wind speed for sustainable turbulence in the nocturnal boundary layer. J Atmos Sci 69(11):3116–3127. https://doi.org/10.1175/JAS-D-12-0107.1

Vignon E, van de Wiel BJ, van Hooijdonk IG, Genthon C, van der Linden SJ, van Hooft JA, Baas P, Maurel W, Traullé O, Casasanta G (2017) Stable boundary-layer regimes at Dome C, Antarctica: observation and analysis. Q J R Meteorol Soc 143(704):1241–1253. https://doi.org/10.1002/qj.2998

van de Wiel B, Moene A, Jonker H, Baas P, Basu S, Donda J, Sun J, Holtslag A (2012) The minimum wind speed for sustainable turbulence in the nocturnal boundary layer. J Atmos Sci 69(11):3116–3127. https://doi.org/10.1175/JAS-D-12-0107.1